# A novel energy-based phase field model for ferrodroplet deformation and breakup in a uniform magnetic field

**Feng Bai[1], Rui Li[2], Xiaofeng Yang[3], Xiaoming He[4]† and Cheng Wang[5]**

[1]School of Mechanical Engineering, Shanghai Jiao Tong University, Shanghai 200240, China

[2]School of Mathematics and Statistics, Xi'an Jiao Tong University, Xi'an 710049, China

[3]Department of Mathematics, University of South Carolina, Columbia, South Carolina 29208, USA

[4]Department of Mathematics and Statistics, Missouri University of Science and Technology, Rolla, Missouri, 65409, USA

[5]Department of Mechanical and Aerospace Engineering, Missouri University of Science and Technology, Rolla, Missouri, 65409, USA

(Received xx; revised xx; accepted xx)

In this paper, we propose a novel, thermodynamically consistent phase field model to simulate the deformation and breakup of a ferrodroplet that is immersed in a viscous medium and subject to an applied uniform magnetic field. Instead of using the magnetic body force in the traditional Rosensweig model, the key idea of this model is to propose a new magnetic energy that enables direct effects of the magnetic field on the interface evolution. The model can thereby be derived from the variational principle via minimizing the free energy of the total system. This energy based modeling idea can be easily extended to include more external fields in a convenient and consistent way for more complicated applications involving multiple external fields. We validate the model by performing a series of numerical simulations, including the comparison with analytic solutions, the investigation of the effect of different types of magnetic fields, the dynamical behaviors of the ferrodroplet breakup under the strong magnetic field, magnetic/velocity/pressure field distributions, the magnetic energy density, and the inertial phenomenon, etc.

**Keywords**: Ferrofluid, Phase Field, Droplet Deformation, Breakup, Finite Element Method, Magnetic Field.



## 1. Introduction

Droplet deformation and breakup dynamics under external forces (e.g., shear) or physical fields (e.g., electric field) are widely studied by many researchers and scientists both experimentally and numerically. Driven by the shear stress of the fluid flow in certain designs of microchannels, the formation/deformation of a droplet can be initiated and the drops can breakup if the shear forces are strong enough (Liu *et al.* (1995); Li *et al.* (2000); De Menech (2006); Yang *et al.* (2006); Menech *et al.* (2008); Müller-Fischer *et al.* (2008); Afkhami *et al.* (2011); Liu *et al.* (2011); Wu *et al.* (2013); Patlazhan *et al.* (2015)). This deformation phenonmena of a drop under external field, mostly under the electric field, are well studied by using different methods to investigate the droplet shape evolutions and variations in the electrohydrodynamics with the effects of inertia, viscosity and nonlinear

† Email address for correspondence: hex@mst.edu

instability (Sherwood (1991); Basaran & Wohlhuter (1992); Hua *et al.* (2008); Salipante & Vlahovska (2010); Lin *et al.* (2012); Yang *et al.* (2013); Lee *et al.* (2014); Lanauze *et al.* (2015); Nganguia *et al.* (2016); Xi *et al.* (2016)). It is found that the droplet will breakup when the applied electric field is over some critical value if the droplet is perfect dielectric (Garton & Krasucki (1964); Torza *et al.* (1971); Paknemat *et al.* (2012); Pillai *et al.* (2015)).

Recently, ferrofluids have become relevant in many applications ranging from engineering to medicine, and have attracted the interests of scientists from many fields due to the fact that these liquids can be controlled directly by the external magnetic field. Ferrofluids are colloidal liquids made of nanoscale ferromagnetic, or ferrimagnetic, nanoscale particles (typically around 10 nanometers in diameter) suspended in a carrier fluid (usually an organic solvent or water) (Rosensweig (1985)). Some traditional applications of such a material include cooling, shaft sealing, shock absorbing, and lubricating (Rosensweig (1985); Raj *et al.* (1995); Odenbach (2004)). More recently, researchers find that the two-phase ferrofluid flow that is composed by ferrofluid and the ambient nonmagnetic medium can be used in micro-technologies and biomedical engineering. For example, hydrophobic ferrofluid droplets have been used for treatment of retinal detachment (Mefford *et al.* (2007)), fluid transport and control (Hatch *et al.* (2001); Hartshorne *et al.* (2004); Mao & Koser (2005); Pal *et al.* (2011)), and sorting of biological cells (Kose *et al.* (2009); Zhu *et al.* (2012); Zeng *et al.* (2013)). In this paper, we are particularly interested in the modeling/simulations of a two-phase incompressible immiscible fluid flow with one phase (droplet) being the ferrofluid, and the other phase (ambient fluid) being the viscous medium. This model can be treated as the simplified version for the prediction and control of a ferrofluid droplet in complex engineering and biomedical applications.

The continuum description of mechanism for the single-phase ferrofluids, known as ferrohydrodynamics (FHD) model, was established by Rosensweig (Rosensweig (1985, 1987)) and Shliomis (Shliomis (1972, 2002)). The Rosensweig's model assumes the ferrofluids to be a linear magnetizable fluids and thus magnetization is collinear with and proportional to the magnetic field. The governing system couples the Navier-Stokes equation and the Maxwell equation, where the effect of polarization force due to material magnetization is regarded as a magnetic body force, which is derived from the magnetic stress tensor, in the momentum equation. The Shliomis' model assumes that the magnetization follows a relaxation equation and it can be considered to be a limiting case of the Rosensweig's model. We refer to Rosensweig (2002, 2007, 1985); Rinaldi & Zahn (2002); Zahn & Greer (1995); Chaves *et al.* (2008); Rosenthal *et al.* (2004) about the PDE/numerical analysis and simulations for the these two models.

To describe the dynamics of two-phase ferrofluid flows, the complete system must include the nonlinear coupling among the following three key ingredients: (i) magnetic field that is governed by the Maxwell equation; (ii) interfacial morphology; and (iii) macroscopic hydrodynamics. The current modeling/numerical simulations for two-phase ferrofluids system is essentially the extension of the existing single-phase FHD models of Rosensweig or Shliomis to the two-phase scenario. Namely, the same magnetic body force term is adopted in the fluid momentum equations while implementing a certain type of interface approach to track the interface between the two phases. Therefore, the main difference among various models/simualtions is essentially the choice of interface tracking approaches, i.e. the sharp interface or the diffusive interface. On one hand, if the interface is described by the sharp interface model where the dynamics of the interface at each time is determined by the so-called Young-Laplace junction condition, then the volume of fluid method, the level set method, or the coupled moving mesh module could be very efficient approaches to solve the model numerically (Korlie *et al.* (2008); Afkhami *et al.*

(2008, 2010); Ki (2010); Ghaffari *et al.* (2015); Rowghanian *et al.* (2016)). On the other hand, if the interface is considered to be diffusive, a robust phase field approach could be a suitable choice to simulate the interfacial dynamics of multiple fluid components.

The phase field method considers the interface as a transition layer where the two fluids mix to a certain degree, governed by a stored mixing energy. The governing equations arise from a standard energetic variational procedure of the Onsager maximum dissipation principle (Onsager 1931*a*,*b*; Lin & Liu 1995, 2001; Berdichevsky 2009; Brenier 1989; Lowengrub & Truskinovsky 1998; Liu & Shen 2003; Hyon *et al.* 2009). Regarding the recent advances in the modeling and numerical analysis for the phase field approach, we refer to Cueto-Felgueroso & Juanes (2014); Menech *et al.* (2008); Du *et al.* (2007); Feng *et al.* (2007, 2016); Feng & Wise (2012); Gal & Grasselli (2011); Guo *et al.* (2014); Kim *et al.* (2004); Kim & Lowengrub (2005); Du *et al.* (2004); Wang *et al.* (2008); Qian *et al.* (2006); Miehe *et al.* (2010); Kim (2012); Liu & Shen (2003); Nochetto *et al.* (2014); Shen & Yang (2009); Wang & Wise (2011); Wise (2010); Yue *et al.* (2004); Zhao *et al.* (2016) and references cited therein. We notice that, the first successful phase field type model has been developed in Nochetto *et al.* (2016) for the two phase ferrofluid flow system, which follows the above traditional approach, i.e., the magnetic body force term is used in the momentum equation.

In this paper, we introduce a novel phase field model to simulate the two-phase ferrofluid flow system. Instead of using the magnetic body force term in the momentum equation, we propose a new magnetic energy and add it to the commonly used Cahn-Hilliard free energy, which is usually composed by the hydrophilic (gradient entropy) and hydrophobic part (nonlinear double well potential) (Onsager (1931*a*,*b*); Lin & Liu (1995, 2001); Berdichevsky (2009); Brenier (1989); Lowengrub & Truskinovsky (1998); Hyon *et al.* (2009)), to demonstrate the magnetic effect that is based on energy balance in the two-phase ferrofluid flow system. This new magnetic energy modifies the traditional Cahn-Hilliard equation, hence directly affects the interface evolution and ferrodroplet deformation. More precisely, through the nonlinear coupling among the stress, the convection and the magnetic field, the system combines the modified Cahn-Hilliard equation with the magnetic energy for the phase field variable, the relaxation equation for magnetization field, the Maxwell equation for the magnetic field, and the Navier-Stokes equation for the hydrodynamics. The general framework of this energy based modeling idea can be easily utilized to include more physics, such as electrohydrodynamics and heat transfer, in a convenient and consistent way for more complicated real world applications involving multiple external fields. We remark that the similar energy had been applied to simulate the liquid crystal deformation and instability in an external physical field, such as electric field or magnetic field, to control the orientation of liquid crystals parallel or normal to the external physical fields by polarization (de Gennes & Prost (1993); Kleman (1983); Lin & Pan (2007); Self *et al.* (2002); García-Cervera & Joo (2015)).

The rest of this paper is organized as follows. In Section 2, we propose the total free energy for the two-phase phase field FHD model and provide the governing system by the variational approach. In Section 3, we will briefly discuss about the non-dimensional parameters, equilibrium shape of ferrodroplet, and other preparation for the numerical experiments. In Section 4, the numerical results of the new model will be discussed systematically for both weak/moderate magnetic fields and strong magnetic fields.

## 2. Theoretical description of the new magnetic energy and phase field equations

We consider a two-phase incompressible, immiscible fluid flow with one phase being the ferrofluid, and the other phase being Newtonian viscous fluid. We use a phase function $\phi(\boldsymbol{x}, t)$ to identify the two Newtonian fluids, namely

$$\phi(\boldsymbol{x}, t) = \begin{cases} 1, & \text{non-ferrofluid phase,} \\ -1, & \text{ferrofluid phase,} \end{cases} \tag{2.1}$$

with a thin, smooth transition region of width $\epsilon$ between the two fluids, so the interface between the two phases is described by the zero level set $\Gamma_t = \{\boldsymbol{x} : \phi(\boldsymbol{x}, t) = 0\}$.

Let $F(\phi) = \frac{1}{4\epsilon^2}(\phi^2 - 1)^2$ be the usual Ginzburg-Landau double-well potential, and define the mixing energy functional

$$E_{mix}(\phi) = \int_\Omega K\Big(\frac{1}{2}|\nabla\phi|^2 + F(\phi)\Big)\, d\boldsymbol{x}, \tag{2.2}$$

where the first term contributes to the hydrophilic type (tendency of mixing) of interactions between the materials and the second part, the double well bulk energy, represents the hydrophobic type (tendency of separation) of interactions. As a consequence of the competition between the two types of interactions, the equilibrium configuration will include a diffusive interface with a thickness proportional to the parameter $\epsilon$. $\Omega$ is the domain in the model system and $K$ is the mixing energy density which is related to the interfacial thickness $\epsilon$ and surface tension $\sigma$ (Yue *et al.* (2004)):

$$\sigma = \frac{2\sqrt{2}}{3}\frac{K}{\epsilon}. \tag{2.3}$$

Based on the existing theoretical studies and experimental observations (Stephen & Straley (1974)), the interface between two-phase ferrofluid flows tends to be parallel to the magnetic field $\mathbf{H}$ for the equilibrium state according to the minimum energy law. This tendency is very similar to the observation from the phenomenon of nematic/smectic liquid crystals under external magnetic field, i.e., the average ellipsoidal molecular tends to be parallel to the magnetic field $\mathbf{H}$ to obtain the equilibrium state (Cowley & Rosensweig (1967); Zelazo & Melcher (1969); Abou *et al.* (2000); Yecko (2009, 2010); Seric *et al.* (2014); Lange *et al.* (2016)). In the nematic/smectic liquid crystals, the magnetic energy is defined as $\int_\Omega -\frac{1}{2}\tilde{\chi}_a(\tilde{\mathbf{n}}\cdot\mathbf{H})^2\, d\boldsymbol{x}$ (Helfrich (1970); Candau *et al.* (1973); Hurault (1973); Napoli & Nobili (2009); García-Cervera & Joo (2012); García-Cervera & Joo (2015)) where $\tilde{\mathbf{n}}$ is the non-dimensionalized average molecular orientation and $\tilde{\chi}_a$ is the magnetic anisotropy.

In contrast to the liquid crystal theory, the effect of magnetic field on the interface of two-phase ferrofluid flows by using phase field method should be demonstrated by the phase field function $\phi$ and the magnetic field $\mathbf{H}$. Compared with the average molecular orientation $\tilde{\mathbf{n}}$, the non-dimensionalized normal vector of interface is expressed as $\epsilon\nabla\phi$. Therefore we propose the new magnetic energy that reads as follows,

$$E_m = \frac{1}{2}\int_\Omega \frac{1}{2}\mu_0(\chi_f - \chi_n)(\epsilon\nabla\phi\cdot\mathbf{H})^2\, d\boldsymbol{x}, \tag{2.4}$$

where $\mu_0$ is a constant representing the magnetic permeability in vacuum and $\chi_f$ and $\chi_n$ are the magnetic susceptibilities of the ferrofluid and non-magnetic fluid respectively with the property $\chi_f - \chi_n > 0$ (Stephen & Straley (1974)). This magnetic energy $E_m$ can

achieve the equilibrium state when $\nabla\phi$ is perpendicular to the applied magnetic field $\mathbf{H}$, which means the interface is parallel to the magnetic field $\mathbf{H}$. The average difference of magnetic permeability at the two-phase smoothly distributed interface can be expressed as $\frac{1}{2}\mu_0(\chi_f - \chi_n) = \frac{1}{2}(\mu_f - \mu_n)$, where $\mu_f$ and $\mu_n$ are the magnetic permeability of the ferrofluids and non-magnetic fluid respectively (Stephen & Straley (1974)), then the new magnetic energy can be rewritten as:

$$E_{mag} = \frac{1}{2}\int_{\Omega} \frac{1}{2}(\mu_f - \mu_n)\epsilon^2(\nabla\phi\cdot\mathbf{H})^2 \; d\boldsymbol{x}. \tag{2.5}$$

Therefore, we obtain the total energy of the hydrodynamic system as a sum of the kinetic energy $E_k$, mixing energy $E_{mix}$ and magnetic energy $E_{mag}$, as follows,

$$\begin{aligned} E_{tot} &= E_k + E_{mix} + E_{mag} \\ &= \int_{\Omega} \Big(\frac{\rho}{2}|\boldsymbol{u}|^2 + K\big(\frac{1}{2}|\nabla\phi|^2 + F(\phi)\big) + \frac{1}{4}(\mu_f - \mu_n)\epsilon^2(\nabla\phi\cdot\mathbf{H})^2\Big) \; d\boldsymbol{x}. \end{aligned} \tag{2.6}$$

where $\rho$ is the density and $\boldsymbol{u}$ is the fluid velocity field. Since the physical properties such as density and viscosity of the two fluid phases vary with phase variable $\phi$, we assume the density $\rho$ and viscosity $\eta$ have the following linear relations with $\phi$,

$$\begin{cases} \rho(\phi) = \dfrac{1}{2}\big((1-\phi)\rho_f + (1+\phi)\rho_n\big), \\ \eta(\phi) = \dfrac{1}{2}\big((1-\phi)\eta_f + (1+\phi)\eta_n\big). \end{cases} \tag{2.7}$$

Here the density of ferrofluid is $\rho_f$ corresponding to $\phi = -1$ and the density of non-magnetic fluid is $\rho_n$ corresponding to $\phi = 1$. The viscosity of ferrofluid is $\eta_f$ corresponding to $\phi = -1$ and the viscosity of non-magnetic fluid is $\eta_n$ corresponding to $\phi = 1$.

Assuming that the phase variable $\phi$ follows the fourth order Cahn-Hilliard dynamics, and the generalized Fick's law that the mass flux be proportional to the gradient of the chemical potential (Jacqmin (1999); Kim (2012)), we derive the following governing system of equations (Abels *et al.* (2012); Shen & Yang (2015); Yue *et al.* (2004)):

$$\begin{cases} w = \dfrac{\delta\left(E_{mix} + E_{mag}\right)}{\delta\phi} = -K(\nabla^2\phi + f(\phi)) - \dfrac{1}{2}(\mu_f - \mu_n)\epsilon^2\nabla\cdot(\nabla\phi\cdot\mathbf{H})\mathbf{H}, \\ \dfrac{\partial\phi}{\partial t} + \boldsymbol{u}\cdot\nabla\phi = M\nabla^2 w, \\ \rho(\dfrac{\partial\boldsymbol{u}}{\partial t} + (\boldsymbol{u}\cdot\nabla)\,\boldsymbol{u}) + J\cdot\nabla\boldsymbol{u} = -\nabla p + \eta\nabla^2\boldsymbol{u} - \phi\nabla w + \boldsymbol{f}_{ext}, \\ \nabla\cdot\boldsymbol{u} = 0, \end{cases} \tag{2.8}$$

with $f(\phi) = F'(\phi)$, $J = -\frac{\rho_1-\rho_2}{2}M\nabla^2 w$, $p$ is the hydrostatic pressure, and $M$ is the mobility parameter that determines the relaxation time of interface and the timescale of diffusion in Cahn-Hilliard equation. $M$ is proportional to the interfacial thickness $M = \chi_{mo}\epsilon^2$, where $\chi_{mo}$ is the mobility tuning parameter (Lim & Lam (2014)). $\boldsymbol{f}_{ext}$ is the external body force such as gravity or buoyancy. In our numerical simulations, we assume no external body or gravity force. The term $\eta\nabla^2\boldsymbol{u}$ represents the effect of viscosity and $-\phi\nabla w$ is the induced body force due to the stress from the combination of the surface tension force and magnetic force.

The multi-physical model includes the following Maxwell equations,

$$\nabla\cdot\mathbf{B} = 0, \quad \nabla\times\mathbf{H} = 0, \tag{2.9}$$

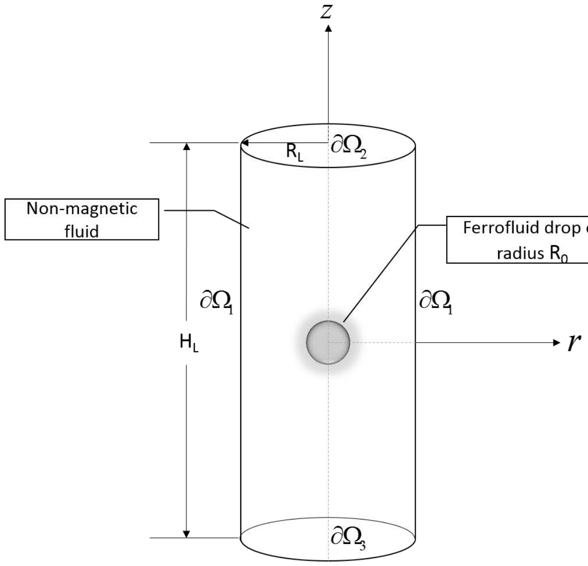


FIG. 1. The 3D schematic of ferrodroplet deformation in an external uniform magnetic field

where $\mathbf{B}$ is the magnetic induction and it can be expressed as:

$$\mathbf{B} = \begin{cases} \mu_f \mathbf{H}, & \text{in ferrofluid} \\ \mu_n \mathbf{H}, & \text{in non-ferrofluid}, \end{cases} \tag{2.10}$$

where the magnetic permeability of the ferrodroplet is $\mu_f = \mu_0(1+\chi_f)$ and the magnetic permeability of the non-magnetic medium is $\mu_n = \mu_0(1+\chi_n)$.

We define a magnetic scalar potential $\psi$ as

$$\mathbf{H} = -\nabla\psi, \tag{2.11}$$

then the Maxwell equation also can be expressed as

$$\begin{cases} -\nabla \cdot (\mu \nabla \psi) = 0, \\ \mu = \dfrac{1}{2}\big((1-\phi)\mu_f + (1+\phi)\mu_n\big), \end{cases} \tag{2.12}$$

where we express the permeability $\mu$ by the phase function $\phi$. Therefore, ((2.8),(2.11),(2.12)) form a closed system with unknowns $\boldsymbol{u}, p, \phi, w, \psi, \mathbf{H}$. We call this system as the magnetic energy-based Cahn-Hilliard-FHD model for two-phase ferrofluid flows. The auxiliary variables $\rho, \eta, \mathbf{B}$ are given by (2.7) and (2.10).

In the following numerical experiments, we set the computational domain $\Omega$ to be a 2D axisymmetric cylinder with the radius $R_L$(=5mm) and the height $H_L$(=20mm), to investigate a ferrodroplet deformation suspended in a nonmagnetic medium. The ferrodroplet is located in the center of the cylindrical geometry with an initial radius $R_0(=1mm)$. The geometric configuration is shown in Fig. 1. We assume the external magnetic field is uniformly distributed in the axisymmetric cylindrical geometry and its direction is pointing from the bottom surface of the cylindrical to the top surface.

The boundary conditions of the system are imposed as follows,

$$\begin{cases} \partial_{\boldsymbol{n}}\psi|_{\partial\Omega_1} = 0, \psi|_{\partial\Omega_2} = 0, \psi|_{\partial\Omega_3} = \psi_b, \\ \partial_{\boldsymbol{n}}\boldsymbol{u}|_{\partial\Omega_1} = 0, \boldsymbol{u}|_{\partial\Omega_2} = \boldsymbol{u}|_{\partial\Omega_3} = 0, \\ \partial_{\boldsymbol{n}}\phi|_{\partial\Omega} = 0, \partial_{\boldsymbol{n}} w|_{\partial\Omega} = 0. \end{cases} \tag{2.13}$$

## 3. Preparation for the numerical experiments

### 3.1. *The dimensionless parameters*

In this subsection, we briefly discuss several dimensionless numbers which will play a key role in the numerical simulation.

It can be seen that the total energy $E_{tot}$ is affected by the interfacial thickness $\varepsilon$ both in the mixing part $E_{mix}$ and the magnetic part $E_{mag}$. In phase field models the interfacial thickness plays a key role in numerical simulations and the sharp interface limit can be demonstrated when the Cahn number $Cn = \varepsilon/R_0 \to 0$. In our study we do not consider the variation of interfacial thickness and it is fixed as $\varepsilon = 0.05R_0$ so that the Cahn number is $Cn = 0.05$.

The equilibrium shape of ferrodroplet is actually determined by the ratio of magnetic effect to surface tension effect, which can be characterized by a dimensionless number—the magnetic bond number (Afkhami *et al.* (2010)):

$$Bo_m = \frac{\mu_0 (H_0)^2}{\sigma \kappa_0} \tag{3.1}$$

where $\mu_0$ is the permeability in vacuum, $H_0$ is the external applied magnetic strength, and $\kappa_0$ is the curvature of the initial un-deformed droplet with radius $R_0$ and $\kappa_0 = 2/R_0$ (Afkhami *et al.* (2010)). When magnetic bond number increases, the magnetic energy will more and more dominate over the surface tension energy so that the interface of the two-phase flows will tend to be parallel to the magnetic field and the ferrodroplet will deform and be elongated significantly.

The Ohnesorge number $Oh = \frac{\eta}{\sqrt{\rho\sigma L}}$ is a dimensionless number representing the viscous effect to the inertial and surface tension effects on small droplets. In our study, the viscous effect will not be investigated since it is not the focus of this article. But the $Oh$ number will be provided in our numerical study.

### 3.2. *Shape of drop equilibrium*

In our study, the deformation of a ferrodroplet in a uniform magnetic field will be numerically investigated by using the new phase field model. And the numerical results will be compared with the well-known analytical solution, which will be shortly recalled in this section. This analytical solution is based on the ellipsoidal shape of ferrodroplet in a uniform magnetic field and could be used to precisely predict the shape of ferrodroplet in weak or moderate magnetic field. For strong magnetic field, the analytical solution tends to be inaccurate and deviate from the experimental results (Afkhami *et al.* (2010); Rowghanian *et al.* (2016)).

The expression of the analytical solution is associated with the aspect ratio $\gamma = b/a$ of deformed ferrodroplet and the magnetic bond number:

$$Bo_m = \left[\frac{1}{\chi} + k\right]^2 \left(\frac{b}{a}\right)^{\frac{1}{3}} \left(2 \cdot \frac{b}{a} - \left(\frac{b}{a}\right)^{-2} - 1\right) \tag{3.2}$$

where $\chi = (\mu_f - \mu_n)/\mu_n$ is the fixed magnetic susceptibility. $2a$ and $2b$ are the minor axis and the major axis of deformed droplet respectively. The parameter $k$ is called demagnetizing factor:

$$k = \left(\frac{1 - E^2}{2E^3}\right) \left(ln \frac{1 + E}{1 - E} - 2E\right) \tag{3.3}$$

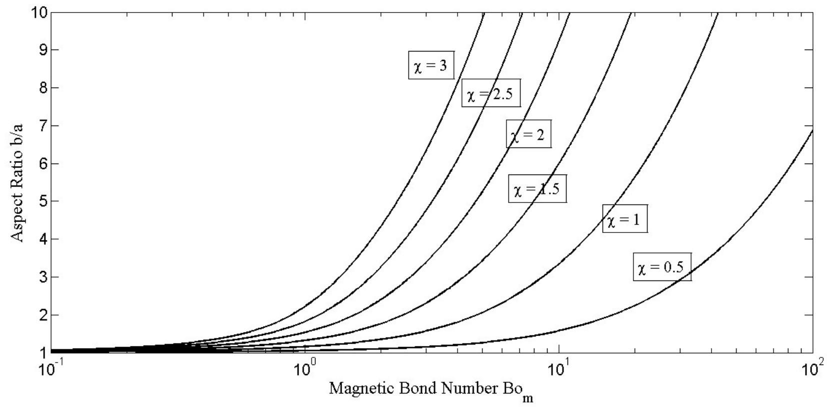


FIG. 2. The aspect ratio at equilibrium as a function of the magnetic bond number at different values of magnetic susceptibility

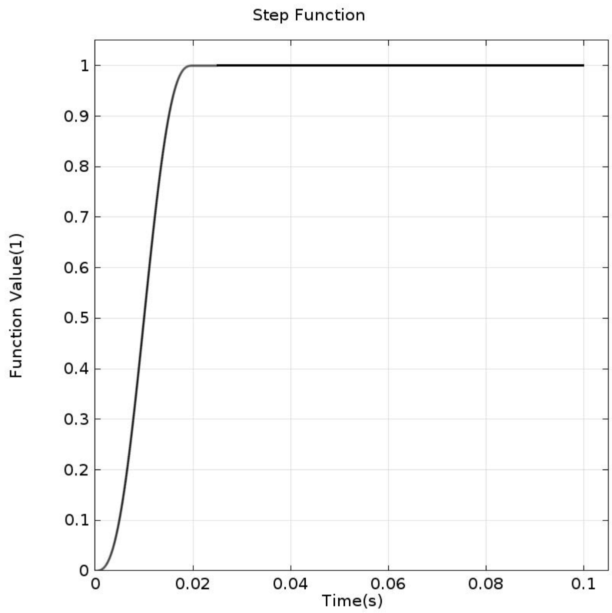


FIG. 3. The step function used in the magnetic boundary condition: the value increases from 0 to 1 in 0.02 second and keeps the value at 1 after the step process(after 0.02 second).

where $E = \sqrt{1 - a^2/b^2}$ is called eccentricity. Fig. 2 shows the aspect ratio $\gamma = b/a$ of ferrodroplet at equilibrium as a function of the magnetic bond number $Bo_m$ with respect to different values of the magnetic susceptibility $\chi$. It can be seen that at low/moderate values of $\chi$, the ferrodroplet deforms continuously and gradually as magnetic field increases.

### 3.3. *Step function of magnetic boundary condition*

In Section 2, we imposed the magnetic boundary condition $\psi|_{\partial\Omega_3} = \psi_b$. In order to qualitatively represent the basic physics procedure in the set-up of the simulation,

a step function is utilized to gradually increase the strength of magnetic field at the bottom boundary in a short period of time at the beginning of the simulation. We choose $\psi_b = \psi_{b0} * \beta(t)$, where $\psi_{b0}$ is the stable magnetic potential after the step process and $\beta(t)$ is illustrated in Fig. 3.

### 3.4. *Numerical implementation of the new phase model and physics parameters*

In the two-phase system we choose Silicone oil as the non-magnetic medium and EMG707 as the ferrofluid. The physical properties are provided as bellows: the density of Silicone oil and EMG707 are $\rho_n = 960(kg/m^3)$ and $\rho_f = 1100(kg/m^3)$ respectively; the viscosity of Silicone oil and EMG707 are $\eta_n = 0.05(Pa * s)$ and $\eta_f = 0.005(Pa * s)$ respectively; the magnetic permeability of Silicone oil and EMG707 are $\mu_n = \mu_0(1 + \chi_n)$ and $\mu_f = (1 + \chi_f)$ respectively, where $\mu_0 = 1.257 \times 10^{-6} \left(N/A^2\right)$ is the magnetic permeability in vacuum; the magnetic susceptibility of Silicone oil and EMG707 are $\chi_n = 0$ and $\chi_f = 1.51$ respectively. The surface tension coefficient between the two phase flows is about $\sigma = 0.025(N/m)$ (Tan *et al.* (2010); Tan & Nguyen (2011)). The mobility in the Cahn-Hilliard equation is determined by the criterion of characteristic mobility $M_c = \chi_{mo}\varepsilon^2$. In Silicone oil - EMG707 two-phase system, the surface tension coefficient is five times of that value in water - mineral oil system. Therefore the characteristic mobility in Silicone oil - EMG707 system is five times of that in water - mineral oil system. Together with $\varepsilon = 0.05R_0$, we have $\chi_{mo} = 0.201(m \cdot s/kg)$.

Since the model configuration is axisymmetric, we simulate the deformation process by using the 2D axisymmetric coordinate (cylindrical coordinate). We use triangle mesh in the 2D axisymmetric system and the size of mesh cells is $0.025R_0$. The total number of 2D triangle mesh cells is about 25,000. Linear finite elements are used to approximate the pressure and quadratic finite elements are used to approximate the other unknowns in the proposed model. The time step we choose is $10^{-4}s$ and the total computational time in our model is $0.1s$.

## 4. Numerical experiments

In this section, we will present a series of numerical results of droplet deformation for two types of magnetic effect: weak/moderate strength and strong strength.

### 4.1. *Droplet deformation at low magnetic bond number and small magnetic permeability*

In this section ferrodroplet deformation of EMG707 in relatively weak magnetic field is numerically studied to investigate the effect of magnetic energy. Based on $\chi_f = 1.51$ for EMG707, we will investigate the effect of different magnetic strength and the evolution of the ferrodroplet with respect to time. We will also investigate the effect of the different values of magnetic susceptibility $\chi_f$.

Fig. 4 shows the 2D cross-section numerical results for the shapes of equilibrium state with four different magnetic bond numbers $Bo_m = 0.1,\ 0.5,\ 1,\ 2$, respectively. The ferrodroplet deformation obeys the minimum energy theory with the increasing magnetic strength. According to the minimum energy theory, the interface of stretched droplet tends to be parallel to the magnetic field to reduce the magnetic energy. On the other hand, the surface energy is proportional to the surface area of the droplet. For a drop of a constant volume, a stretched droplet results in an increasing surface area and surface energy. The surface tension thus tries to restore the drop to spherical shape. The final equilibrium shape is due to the competition of these two effects and will result in a minimum energy of the entire system. The relative strength of the

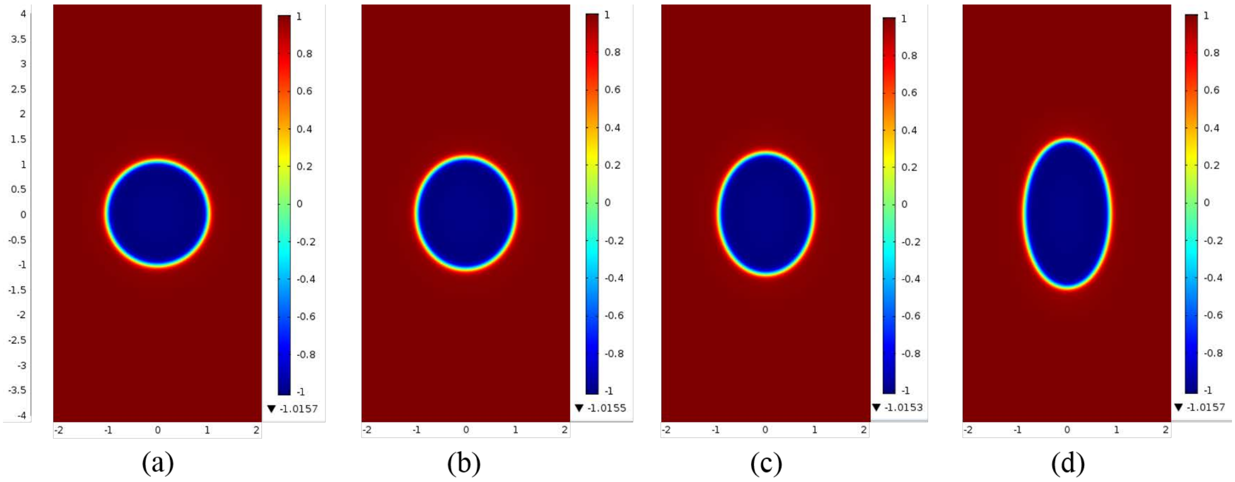


FIG. 4. The shape of ferrodroplet deformation at equilibrium state in Silicone - EMG707 two phase system with four different low magnetic bond numbers at time $T = 0.1s$. (a)$Bo_m = 0.1$, (b) $Bo_m = 0.5$, (c) $Bo_m = 1$, (d) $Bo_m = 2$.

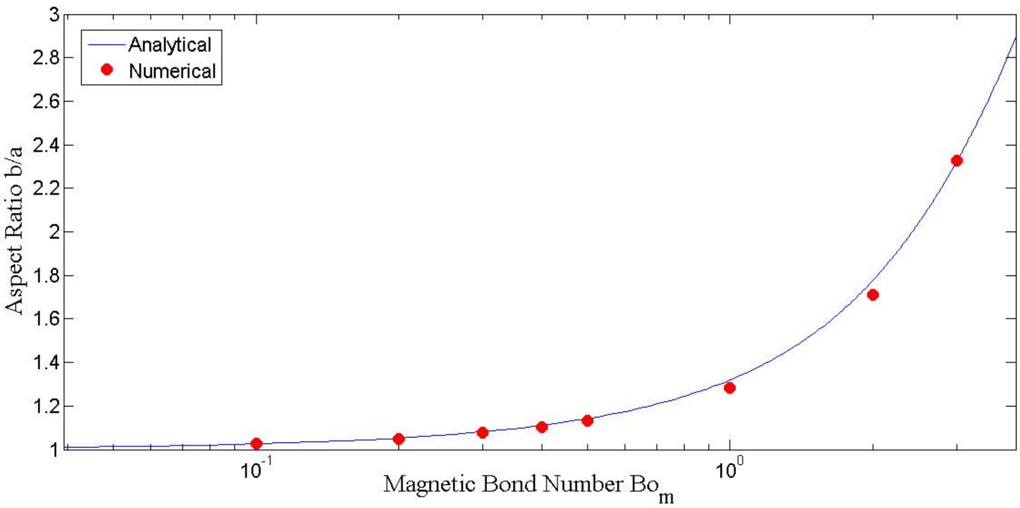


FIG. 5. The comparison between the numerical results and analytical results (see Fig. 2) for the equilibrium state aspect ratio by using physical properties EMG707.

magnetic is characterized by the magnetic bond number. Based on Fig. 2, larger magnetic bond number leads to larger aspect ratio, hence larger deformation corresponding to the increasing magnetic effect over surface tension effect.

Moreover, the numerical results are compared with the analytical solution discussed in section 3.2 to justify our new phase field model. We use the real physical properties of EMG707 with the magnetic permeability $\chi_f = 1.51$. By comparing with the analytical solutions in Fig. 5, it can be seen that the numerical results match the analytical results very well for low/moderate magnetic bond number. This means that our new model is accurate and satisfies the analytical theory of ellipsoidal shape at low magnetic bond number.

In Fig. 6 the equilibrium state of the distribution of magnetic field $\mathbf{H}$ (the left) and the magnetic induction $\mathbf{B}$ (the right) are shown with two magnetic bond numbers $Bo_m = 0.1$ and $Bo_m = 2$. According to the magnetic boundary conditions, the directions of magnetic field and induction are pointing from the bottom to the top, which is shown by the arrows in the right half. In the left half the magnetic field strength reaches the maximum values on the bottom and top sides of the ferrodroplet and the low magnetic strength occurs

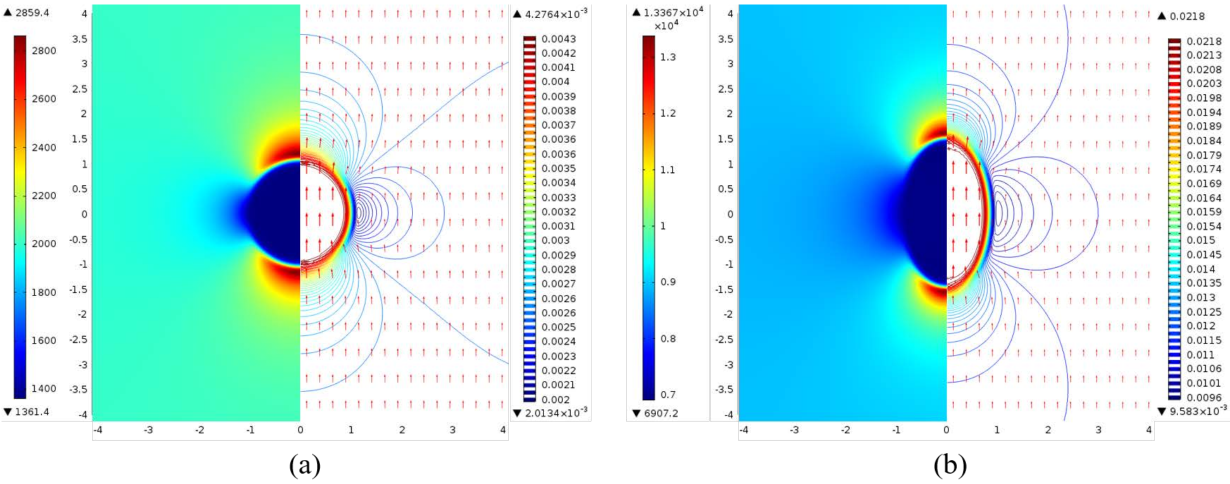

FIG. 6. The distribution of magnetic field strength and induction at two magnetic bond numbers in Silicone - EMG707 system. (a)$Bo_m = 0.1$ and (b)$Bo_m = 2$. The left parts of the two depicts show the magnetic field strength. The contours in right parts of show the gradients of the magnetic induction and the arrows show the direction and relative strength of magnetic induction **B**.

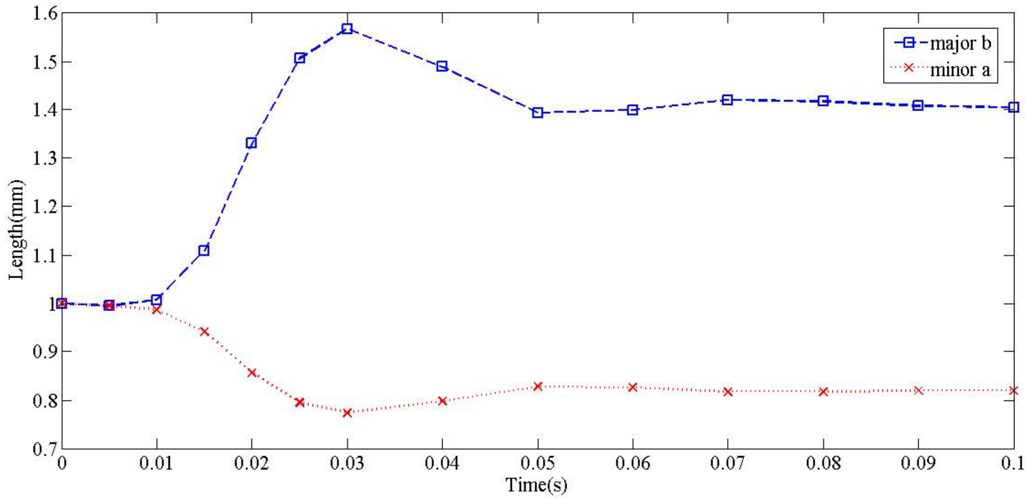


FIG. 7. The evolution of semi-major axis $b$ and semi-minor axis $a$ in the time span of $0s \sim 0.1s$. The magnetic bond number is $Bo_m = 2$.

inside the droplet since the magnetic permeability in the ferrodroplet is larger than that of the ambient non-magnetic medium. In the non-uniform distribution of the solution, one can easily see the fast change in the interfacial region since the magnetic permeability $\mu = \frac{1}{2}[(1-\phi)\mu_f + (1+\phi)\mu_n]$ changes quickly in the interfacial region. These results are also similar to those of Afkhami *et al.* (2010). Furthermore, comparing the two graphs in Fig. 6, the maximum difference of magnetic strength between the inside and outside of the ferrodroplet becomes larger with the increasing magnetic bond number.

Even though the shape of ferrodroplet finally reaches an equilibrium state, the dynamic deformation is observed in the numerical simulation and it is found that the inertia phenomenon should not be neglected in the deformation process. From Fig. 7, one can easily see the effect of the inertia phenomenon: the semi-major axis and semi-minor axis first reach peak values and then converge to the steady state values. In this system, the Ohnesorge number, which represents the viscous force over the inertia and surface tension force, is $Oh = \frac{\eta}{\sqrt{\rho\sigma L}} \approx 0.225$.

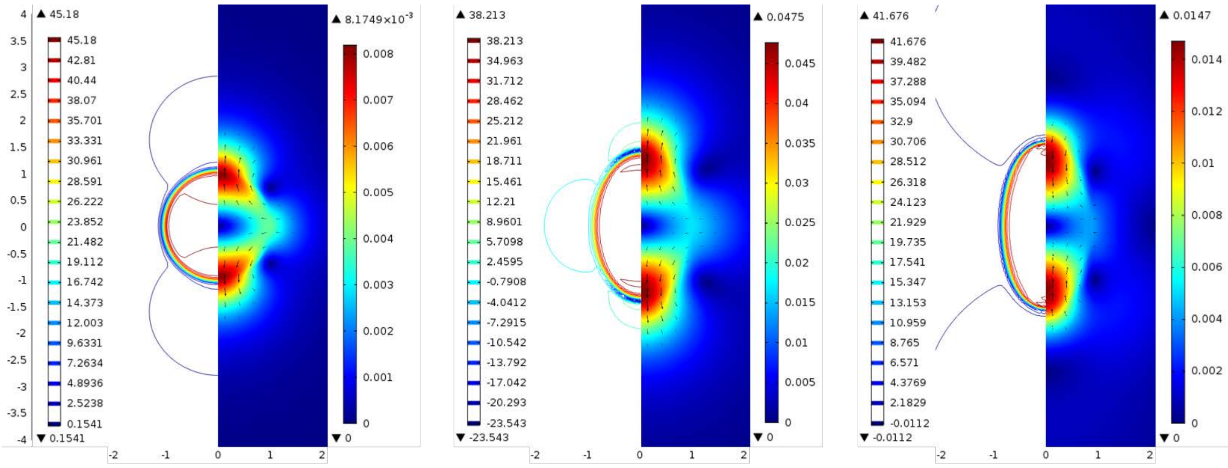


(a) (b) (c)

FIG. 8. The velocity and pressure distribution at three different time instances in the Silicone - EMG707 system. (a)$T = 0.01s$, (b)$T = 0.02s$, (c)$T = 0.04s$.

In typical lab experiments, the ferrodroplets may be opaque and the internal flows may be difficult to visualize and measure. Thus, the numerical simulations could provide valuable insights on the detailed flow velocity fields. In Fig. 8, The velocity and pressure distribution at three different time instances are shown. The magnetic bond number is $Bo_m = 2$. Both the velocity field and the pressure distribution are symmetric along the coordinate $r = 0$. Hence we only provide half of the plots for them. The left parts of plots are contour plot of pressure and the right parts are velocity field. The color represents the magnitude of the velocity and the arrows show the direction of the velocity. At time $T = 0.01s$ the deformation in the vertical direction is relative small since the magnetic field begins to be increased from 0. The velocity magnitude reaches its maximum at the bottom and top of the ferrodroplet but almost 0 in the center of ferrodroplet. At time $T = 0.02s$ the ferrodroplet further deforms in the vertical direction with the increasing magnetic field and the shape comes to an ellipsoid with $b = 1.331mm$ and $a = 0.857mm$. The magnitude of velocity significantly increases near the bottom and top of the ferrodroplet. At time $T = 0.04s$ the semi-major axis $b$ shrinks and the semi-minor axis $a$ regrows. This can be easily observed from the arrow direction which is opposite to that of other plots.

Now we investigate the effect of the different values of magnetic susceptibility $\chi_f$ and bond number $Bo_m$ by using the same physical properties of the Silicone-EMG707 system except $\chi_f$. Three different values of magnetic permeability $\chi = 1$, $\chi = 2$ and $\chi = 3$ are used in our model for numerical tests and the results are compared with analytical solutions in Fig. 9. All the numerical results are the equilibrium state at time $T = 0.1s$. The results show that our numerical solutions well match the analytical solutions with the increasing magnetic bond number from $Bo_m = 0.1$ to $Bo_m = 1$ and magnetic susceptibility from $\chi = 1$ to $\chi = 3$. When the magnetic susceptibility and magnetic bond number become large enough, the magnetic field may become strong enough so that the droplet may break up, hence cause the analytic solution to be inaccurate and deviate from the experimental results (Afkhami *et al.* (2010); Rowghanian *et al.* (2016)). Therefore, we do not compare the numerical solution with the analytic solution for this case in this section, but discuss about the details of the droplet breakup in the next section.

On the other hand, the magnetic energy density distribution ($e_m = \mid \frac{1}{2}\mu\mathbf{H}^2 \mid$) under three different conditions are presented in Fig. 10. It can be seen that the magnetic

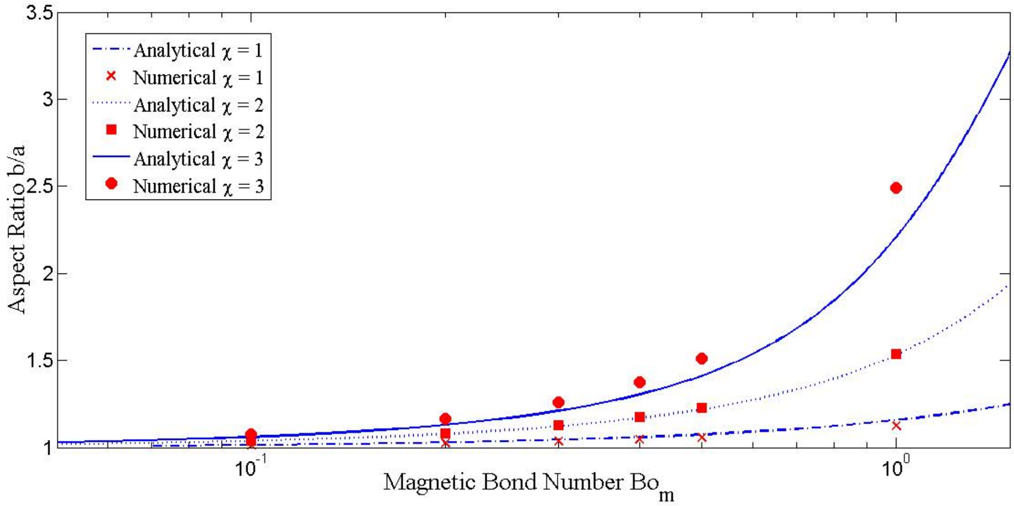


FIG. 9. The comparison of equilibrium drop aspect ratio between numerical and analytical results for three different values of magnetic permeability at low magnetic bond numbers. Other physical properties of the ferrodroplet are the same as EMG707.

energy density reaches its maximum at top/bottom of the ferrodroplet and its minimum at left/right of the ferrodroplet. We can also find that the magnetic energy increases when $Bo_m$ and $\chi$ increase: the maximum energy density is $e_m = 47J/m^3$ for $\chi = 1, Bo_m = 1$, $e_m = 96J/m^3$ for $\chi = 3, Bo_m = 1$, and $e_m = 257.5J/m^3$ for $\chi = 1, Bo_m = 5$, which indicates that the magnetic energy is proportional to magnetic field strength.

To investigate the dynamic magnetic energy variation during the deformation process of the ferrodoplet, we present the energy plots at various time steps in Fig. 11 for $\chi = 3$ and $Bo_m = 1$. It can be seen that the magnetic energy density is almost uniform at the beginning and the end, but non-uniform when the deformation is large enough during the procedure. The larger deformation corresponds to more obvious non-uniform distribution. In the non-uniform magnetic energy density, the magnitude is larger in the center of ellipsoidal ferrodroplet than the bottom/top inside the droplet.

### 4.2. *Droplet deformation and breakup at high magnetic bond number and magnetic permeability*

As reviewed in the introduction, the traditional Rosensweig model based on the magnetic stress tensor on the interface of droplet is used to simulate the ferrodroplet deformation in uniform magnetic field (Afkhami *et al.* (2010); Rowghanian *et al.* (2016)). The ferrodroplet deforms and is stretched along the direction of magnetic field and the aspect ratio $b/a$ of deformed shape increases with increasing magnetic field strength. These simulations are found to be reasonable and match the analytical solutions at low to moderate magnetic bond number.

As discussed above, when the magnetic effect is strong enough with high magnetic bond number or magnetic permeability, it is expected that the ferrodroplet can be broken up (Garton & Krasucki (1964); Torza *et al.* (1971); Sherwood (1988); Sofonea *et al.* (2002); Paknemat *et al.* (2012); Pillai *et al.* (2015)). Since the analytic solution (3.2) is true only when the ferrodroplet keeps the ellipsoid shape, it cannot be used for the procedure of the large deformation and breakup of ferrodroplet. Therefore, in this subsection, we will utilize our new phase field model, which is based on the minimum energy law and the newly introduced magnetic energy, to investigate the large deformation and breakup process.

From Fig. 12 (2D cross-section results) and Fig. 13 (3D results), it can be seen that

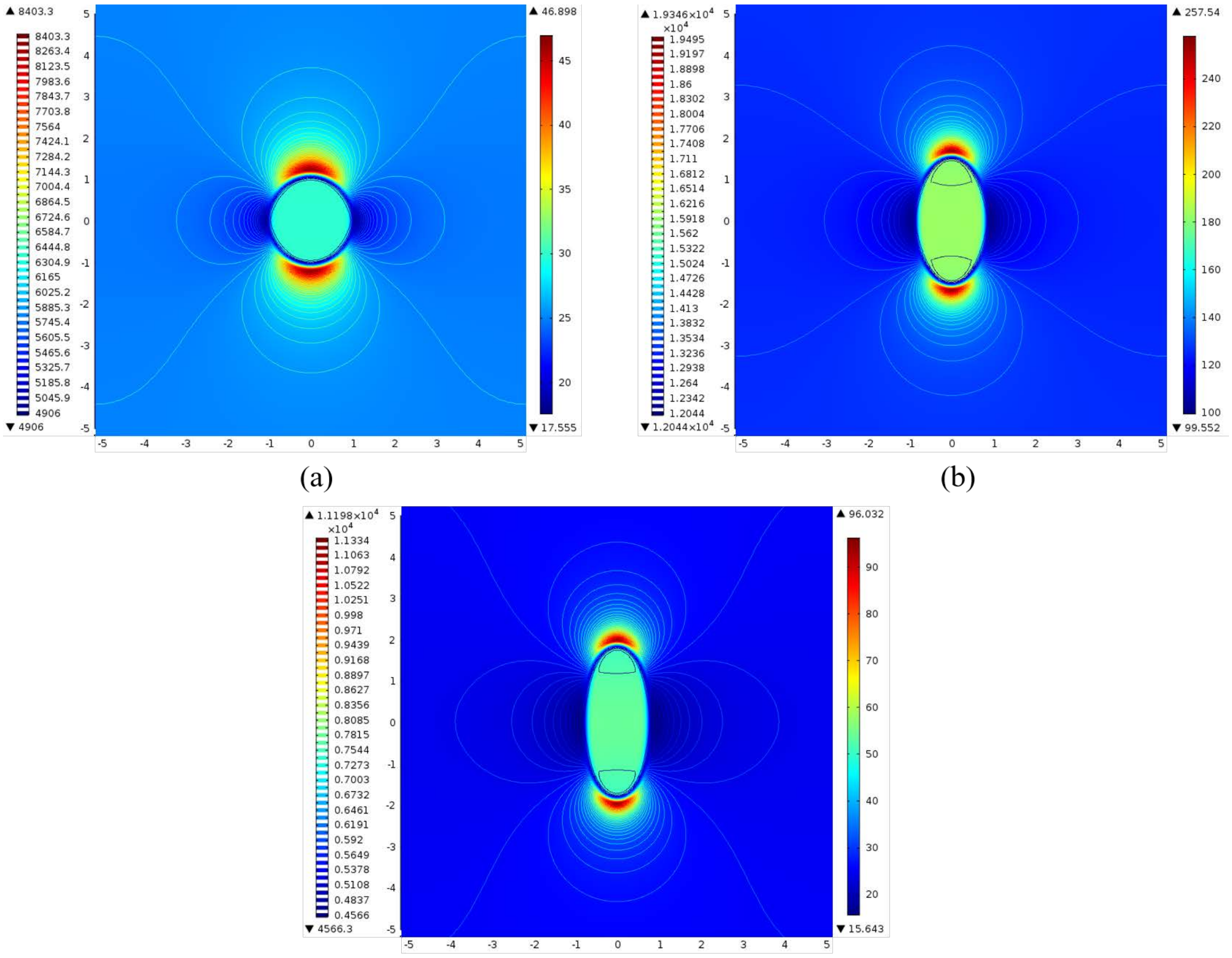

(a) (b) (c)

FIG. 10. The magnetic energy density distributions in the final equilibrium state $T = 0.1s$ with three different magnetic conditions: (a)$\chi_f = 1, Bo_m = 1$, (b)$\chi_f = 1, Bo_m = 5$ and (c)$\chi_f = 3, Bo_m = 1$. The contour distributions shown are the magnetic field strength.

the ferrodroplet deforms very fast in a short time from $T = 0.01s$ to $T = 0.03s$ since the magnetic bond number is large compared with the numerical experiments in the previous subsection. After $T = 0.03s$ the middle part of the droplet starts to shrink and becomes narrower and narrower until the droplet breaks up around $T = 0.07s$. The shapes of ferrodroplet in this procedure do not satisfy ellipsoid assumption for the analytical solutions (3.2). Hence this analytical solution cannot be used to predict this breakup phenomenon. The breakup of the drop can be explained by whether there exists an equilibrium and stable shape to satisfy minimization of the system energy. For weak/moderate magnetic field, it is possible for the surface energy of the drop to overcome the decreasing of magnetic energy. For strong magnetic field, the magnetic energy is much stronger, and the drop has to breakup in order to increase the overall surface area and thus surface energy.

Since the ferrodroplet deformation and breakup process is caused by the external magnetic field, magnetic field and induction are the key points to determine the deformation and breakup process. For different time instances, Fig. 14 shows the magnetic field strength in the left part and the magnetic induction in the right part for the Silicone - EMG707 system with the magnetic bond number $Bo_m = 5$. Compared with Fig. 6, both the magnetic field and induction are not uniform, especially when the droplet starts to shrink at its middle part. The magnetic field and induction around the middle part are

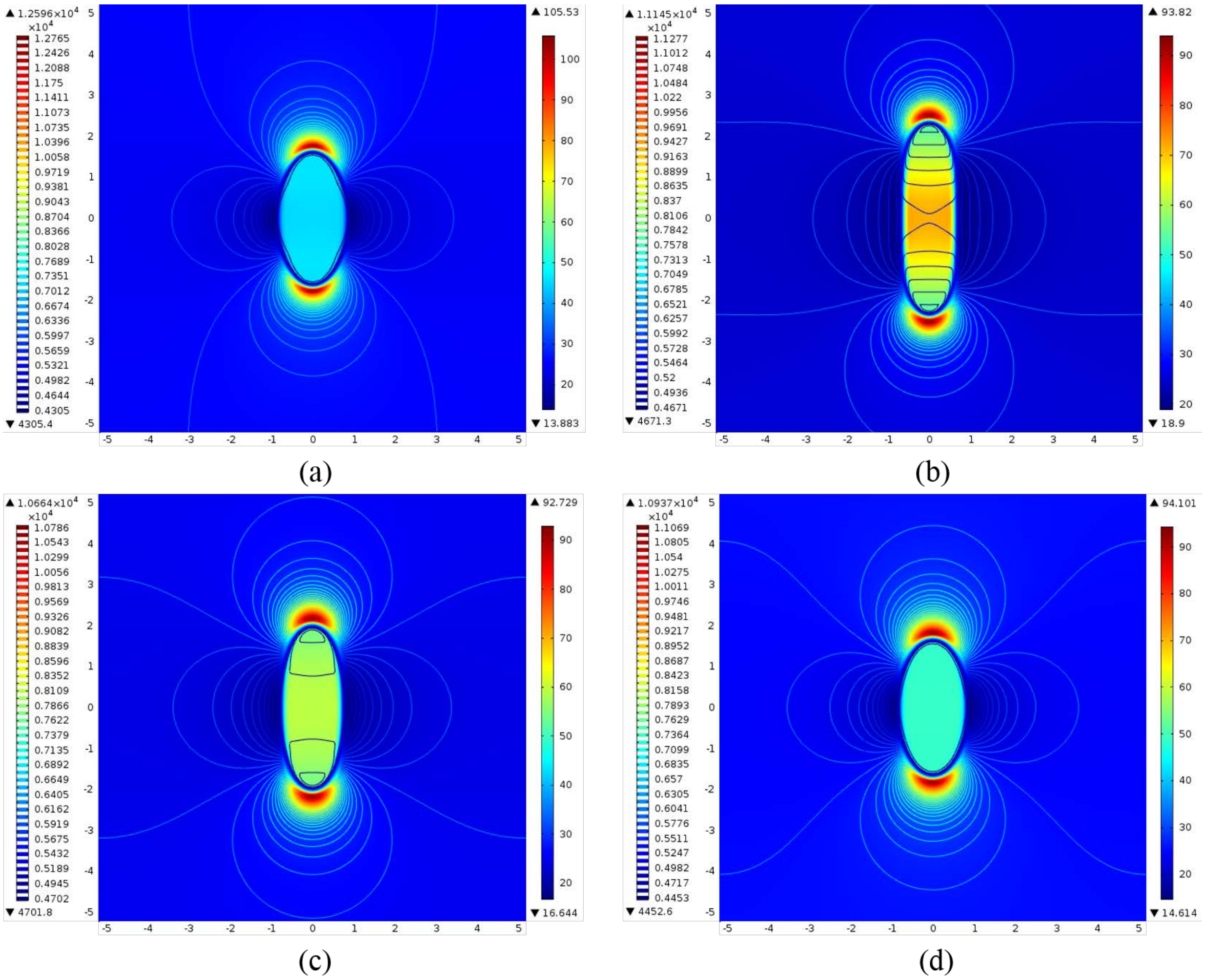


FIG. 11. The dynamic deformation process of magnetic energy density in the condition of $\chi_f = 3, Bo_m = 1$ at four different time instances (a)$T = 0.02s$, (b)$T = 0.04s$, (c)$T = 0.06s$, (d)$T = 0.08s$. The contour distributions shown are the magnetic field strength.

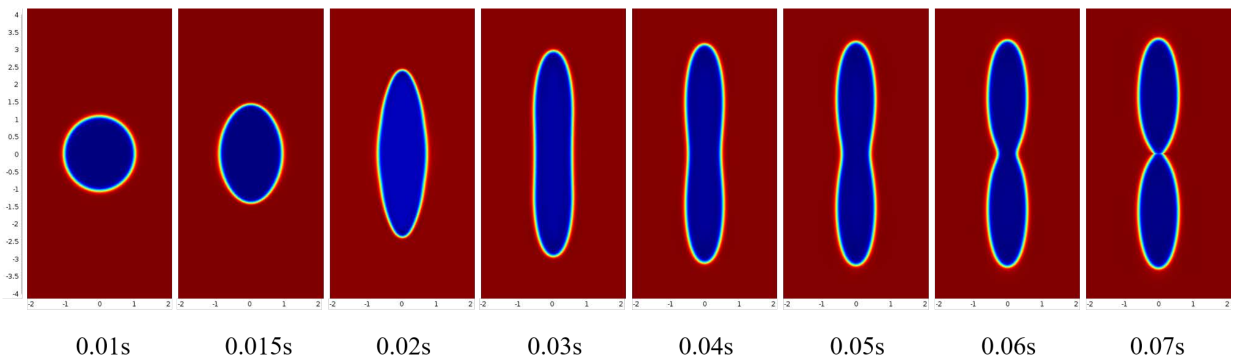


FIG. 12. 2D cross section of ferrodroplet deformation and breakup at magnetic bond number $Bo_m = 5$ in Silicone - EMG707 system. The magnetic permeability $\chi_f = 1.51$. From left to right $T = 0.01s \sim 0.07s$. We use the step function to increase magnetic field in time span of $0s \sim 0.02s$

much higher than those of the rest of the ferrodroplet. This is one of the key reasons to cause the breakup of the ferrodroplet.

In Fig. 15, the velocity and pressure distributions are provided. Compared with Fig. 8, the pressure distribution is more non-uniform. When the droplet begins to shrink in its middle part, the velocity distribution also significantly changes since the maximum flow

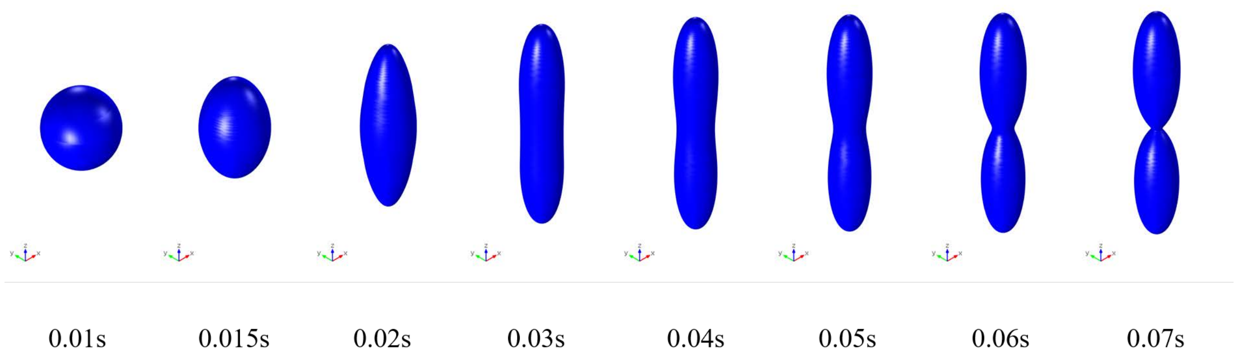


FIG. 13. 3D results of ferrodroplet deformation and breakup at magnetic bond number $Bo_m = 5$ in Silicone - EMG707 system. The magnetic permeability $\chi = 1.51$. From left to right $T = 0.01s \sim 0.07s$. We use the step function to increase magnetic field in time span of $0s \sim 0.02s$

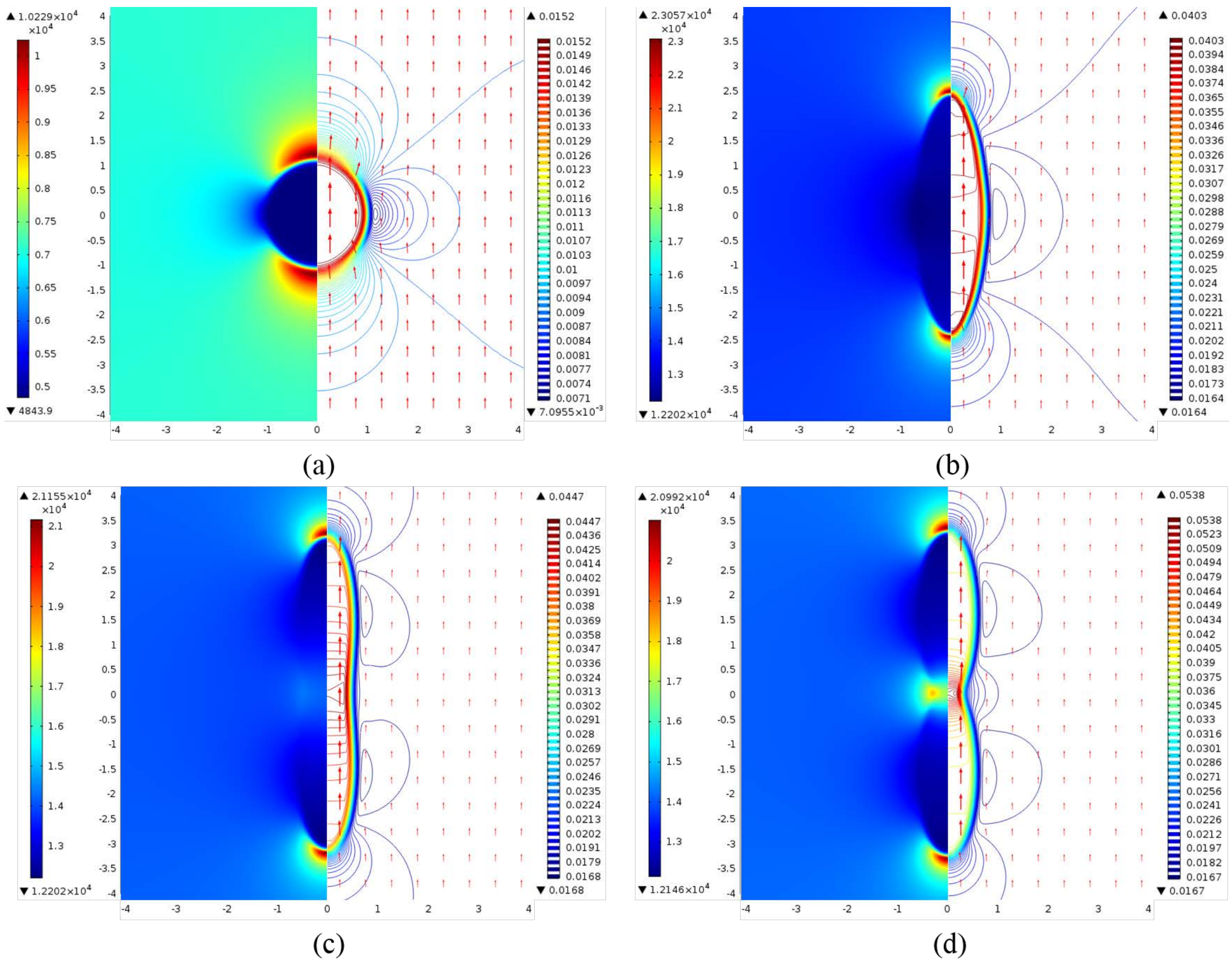


FIG. 14. Magnetic field and induction distribution with time in the deformation and breakup process for Silicone - EMG707 system. The color distribution is magnetic field strength. The contours and arrows represent the strength and direction of magnetic induction. (a)$T = 0.01s$, (b)$T = 0.02s$, (c)$T = 0.04s$, (d)$T = 0.06s$

speed area tends to move to the middle part of ferrodroplet. Meanwhile, the flow speed of the bottom/top parts of the droplet significantly decreases to a much lower value than the surrounding area.

Another critical physical quantity to determine the droplet deformation and breakup is the magnetic energy density. Hence the magnetic energy density distributions at different

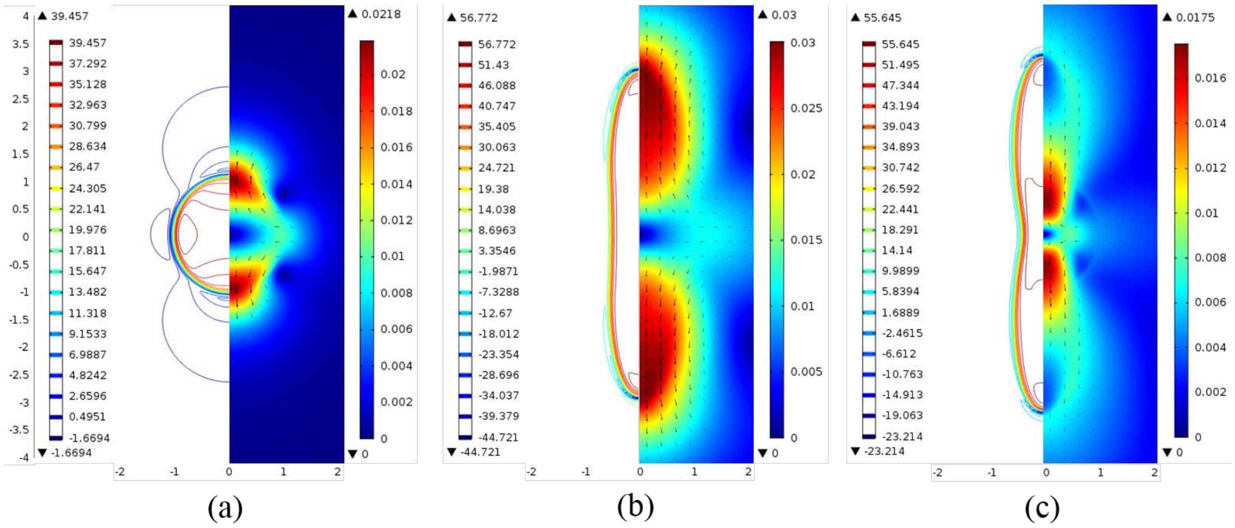

FIG. 15. The velocity and pressure distributions of ferrodroplet in the deformation and breakup process in Silicone - EMG707 system($\chi_f = 1.51, Bo_m = 5$). (a)$T = 0.01s$, (b)$T = 0.03s$, (c)$T = 0.05s$, the left parts are pressure contour lines and the right parts are velocity color distributions

time steps in the deformation and breakup process with magnetic bond number $Bo_m = 5$ are shown in Fig. 16. The the distribution at initial time is similar to the results at low magnetic bond number part (a) in Fig. 10. It can be clearly observed that in a short time the magnetic energy density becomes more nonuniform inside the ferrodroplet. When the middle part of the droplet shrinks, the energy density concentrate more around the middle part of the droplet. This is another key reason to cause the breakup of the ferrodroplet.

Finally we investigate the effect of different values of the magnetic permeability. In Fig. 17 the energy density plots are provided for $\chi_f = 3$, $\chi_f = 4$ and $\chi_f = 5$. It can observed that the larger $\chi_f$ leads to the breakup of the droplet and a longer droplet when it's broken up. It is found that the half of droplet length is about $L = 2.29mm$, $L = 3.47mm$ for $\chi_f = 4$ and $L = 4.04mm$ for $\chi_f = 5$, which indicates that the large deformation and breakup length is correlated with large magnetic permeability. Furthermore, the magnetic energy density increases with the magnetic permeability, especially around the breakup area. In Fig. 18 the variation of semi-major axis $b$ and semi-minor axis $a$ with respect to time is shown. Obviously, the higher values of $\chi_f$ lead to larger semi-major axis and smaller semi-minor axis. The breakup can happen only when $\chi_f$ is large enough. One can also see the inertia phenomenon for $\chi_f = 3$, which is similar to that for $\chi_f = 1.51$ of Fig. 7.

## 5. Conclusions

In this paper a novel phase field model of ferrodroplet deformation was proposed based on minimum energy law and the numerical results in 2D axisymmetric coordinate system were discussed. The key modeling idea is to add a new magnetic energy to the commonly used Cahn-Hilliard free energy, instead of using the magnetic body force term in the momentum equation which is the traditional modeling technique in the literature. Based on this novel idea, we proposed the magnetic energy-based Cahn-Hilliard-FHD model (2.7)-(2.12)) for two-phase ferrofluid flows. In the numerical experiments, we first investigated the deformation process of ferrodroplet for low magnetic bond number and small permeability numerically by using our new model and compared the numerical results with the well-known analytical solutions to justify the new model. Moreover,

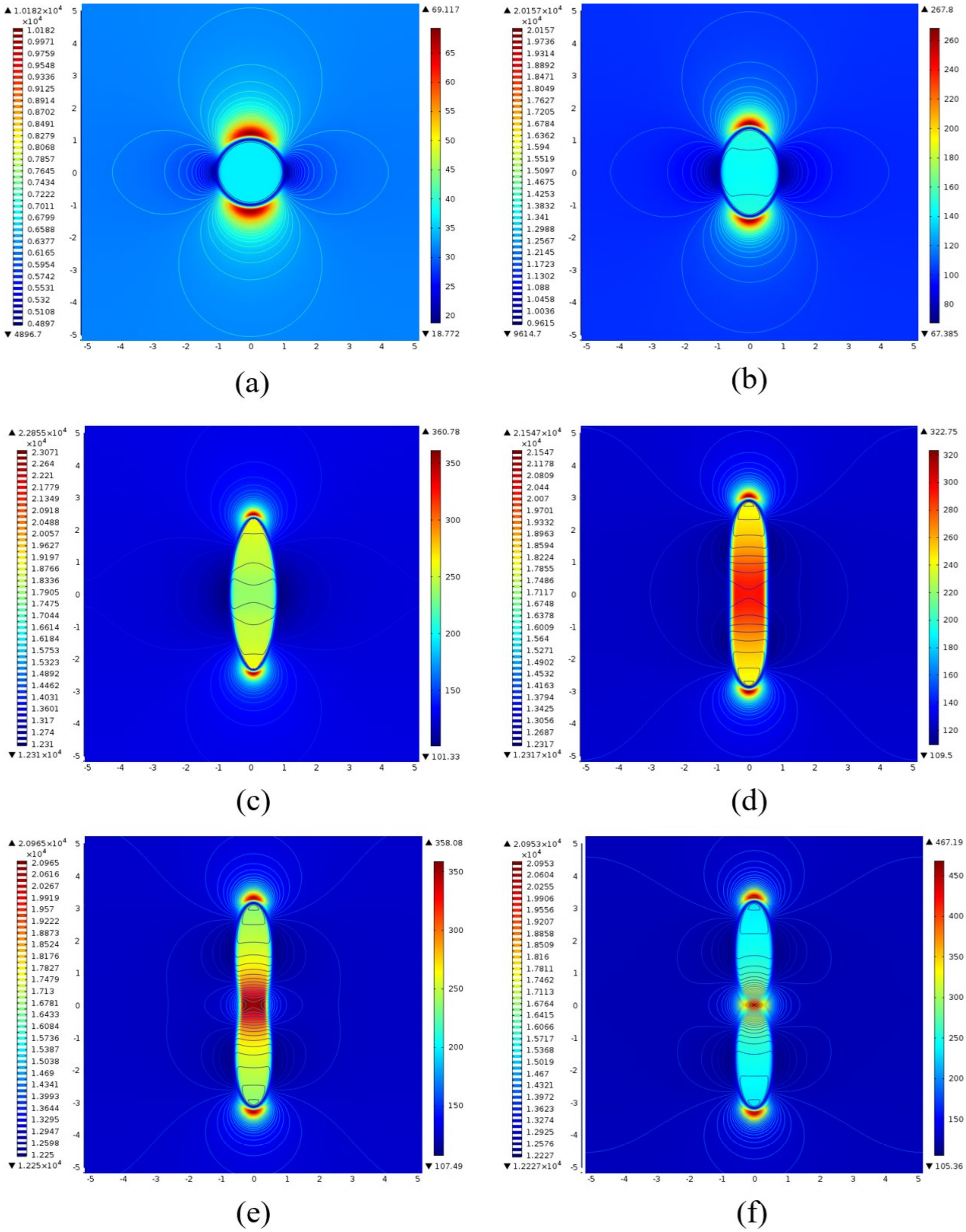


Fig. 16. The evolution of magnetic energy density distributions in breakup process in Silicone - EMG707 system($\chi_f = 1.51, Bo_m = 5$) with time instances. (a)$T = 0.01s$, (b)$T = 0.015s$, (c)$T = 0.02s$, (d)$T = 0.03s$, (e)$T = 0.05s$, (f)$T = 0.06s$. The contour lines represent the magnetic field strength and the magnetic energy density is expressed in the color pics.

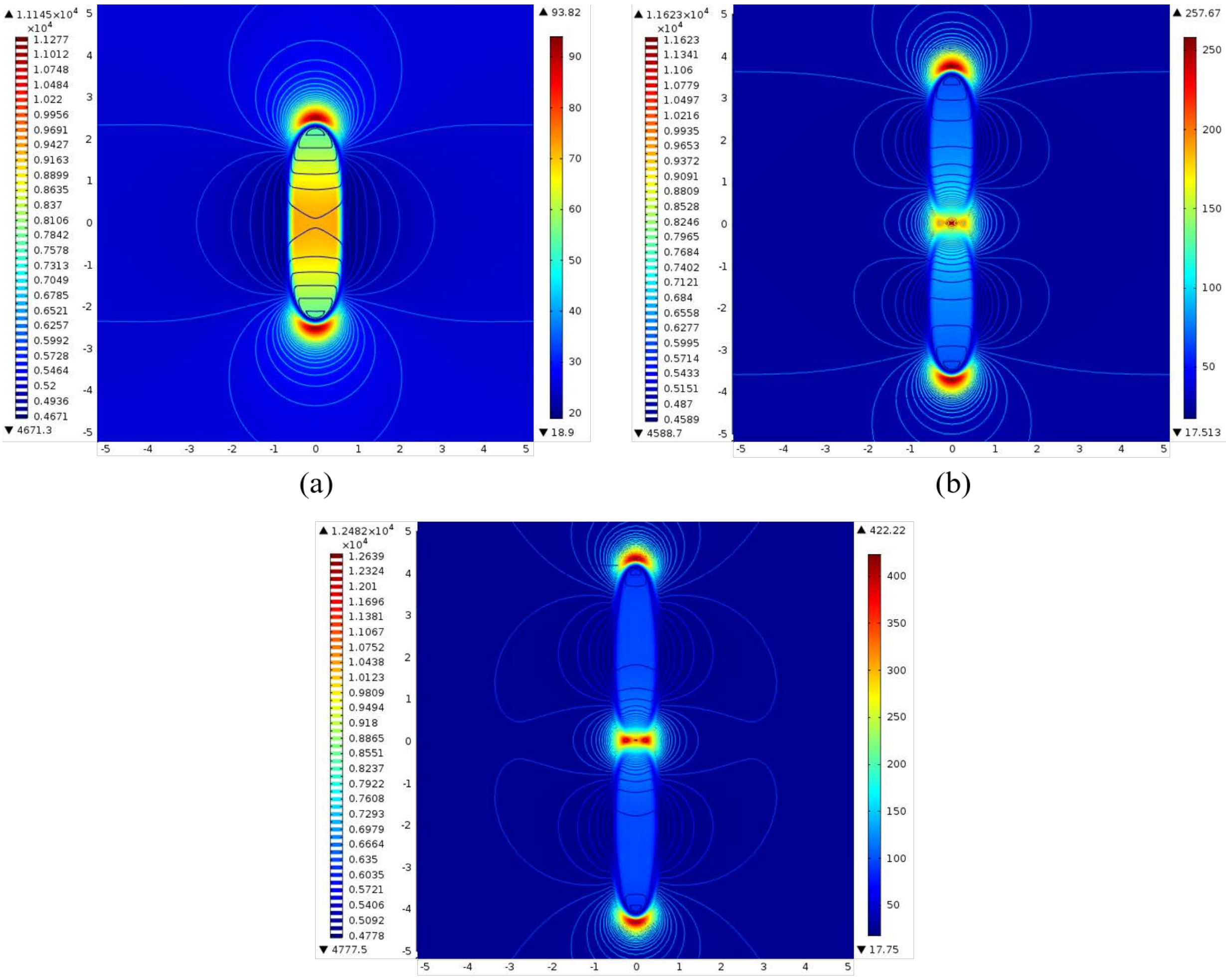

(a) (b) (c)

Fig. 17. The magnetic energy density distribution in the large deformation and breakup of ferrodroplet for different magnetic permeability (a)$\chi_f = 3$, (b)$\chi_f = 4$ and (c)$\chi_f = 5$. The magnetic bond number $Bo_m = 1$ and other physical properties of the ferrodroplet are used as EMG707. The contour lines represent the magnetic field strength and the magnetic energy density is expressed in the color pics.

the newly proposed model is utilized to investigate the effect of the higher magnetic bond number and magnetic permeability, which may cause the droplet breakup when the magnetic field is strong enough. In both numerical experiments, the magnetic field strength, velocity and pressure distribution, evolution of ferrodroplet shape with respect to time, and magnetic energy density are discussed to demonstrate the deformation and breakup process.

## 6. Acknowledgement

This work is partly supported by the U.S. National Science Foundation under grant numbers DMS-1200487 and DMS-1418898, National Natural Science Foundation of China under grant numbers 51376129 and 51036005.

REFERENCES

Abels, H., Garcke, H. & Grün, G. 2012 Thermodynamically consistent, frame indifferent diffuse interface models for incompressible two-phase flows with different densities. *Math. Models Methods Appl. Sci.* **22** (3), 1150013.

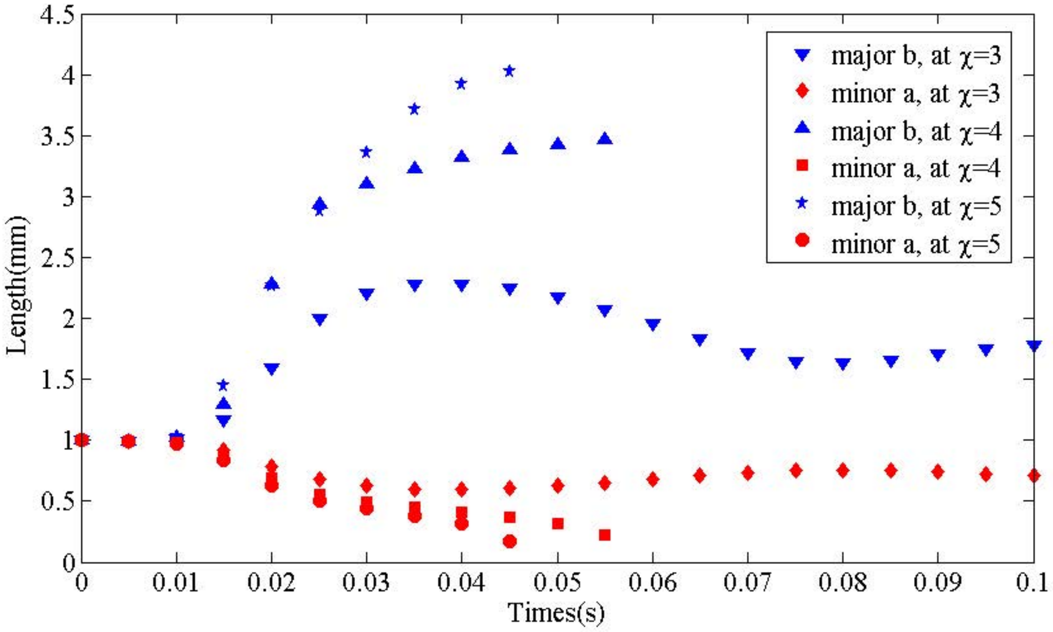


FIG. 18. The variation of major $b$ and minor $a$ with time at three different values of magnetic permeability ($\chi_f = 3$, $\chi_f = 4$ and $\chi_f = 5$). Other physical properties of the ferrodroplet are the same as EMG707. Magnetic bond number is $Bo_m = 1$ and time span is $T = 0s \sim 0.1s$

ABOU, B., WESFREID, J. E. & ROUX, S. 2000 The normal field instability in ferrofluids: hexagonsquare transition mechanism and wavenumber selection. *J. Fluid Mech.* **416**, 217–237.

AFKHAMI, S., LESHANSKY, A. M. & RENARDY, Y. 2011 Numerical investigation of elongated drops in a microfluidic T-junction. *Phys. Fluids* **23** (2), 022002.

AFKHAMI, S., RENARDY, Y., RENARDY, M., RIFFLE, J. S. & ST. PIERRE, T. G. 2008 Field-induced motion of ferrofluid droplets through immiscible viscous media. *J. Fluid Mech.* **610**, 363–380.

AFKHAMI, S., TYLER, A. J., RENARDY, Y., RENARDY, M., ST. PIERRE, T. G., WOODWARD, R. C. & RIFFLE, J. S. 2010 Deformation of a hydrophobic ferrofluid droplet suspended in a viscous medium under uniform magnetic fields. *J. Fluid Mech.* **663**, 358–384.

BASARAN, O. A. & WOHLHUTER, F. K. 1992 Effect of nonlinear polarization on shapes and stability of pendant and sessile drops in an electric (magnetic) field. *J. Fluid Mech.* **244**, 1–16.

BERDICHEVSKY, V. L. 2009 Variational principles of continuum mechanics: I. fundamentals (interaction of mechanics and mathematics).

BRENIER, Y. 1989 The least action principle and the related concept of generalized flows for incompressible perfect fluids. *J. Am. Math. Soc.* **2**, 225–255.

CANDAU, S., P. LE ROY & DEBEAUVAIS, F. 1973 Magnetic field effects in nematic and cholesteric droplets suspended in a isotropic liquid. *Mol. Cryst. Liq. Cryst.* **23** (3-4), 283–297.

CHAVES, A., ZAHN, M. & RINALDI, C. 2008 Spin-up flow of ferrofluids: Asymptotic theory and experimental measurements. *Phys. Fluids* **20**, 053102.

COWLEY, M. D. & ROSENSWEIG, R. E. 1967 The interfacial stability of a ferromagnetic fluid. *J. Fluid Mech.* **30** (04), 671–688.

CUETO-FELGUEROSO, L. & JUANES, R. 2014 A phase-field model of two-phase Hele-Shaw flow. *J. Fluid Mech.* **758**, 522–552.

DE MENECH, M. 2006 Modeling of droplet breakup in a microfluidic T-shaped junction with a phase-field model. *Phys. Rev. E* **73**, 031505.

DU, Q., LI, M. & LIU, C. 2007 Analysis of a phase field Navier-Stokes vesicle-fluid interaction model. *Discrete Contin. Dyn. Syst. Ser. B* **8** (3), 539–556.

Du, Q., Liu, C. & Wang, X. 2004 Phase field approach in the numerical study of the elastic bending energy for vesicle membranes. *J. Comput. Phys.* **198**, 450–468.

Feng, X., He, Y. & Liu, C. 2007 Analysis of finite element approximations of a phase field model for two-phase fluids. *Math. Comp.* **76** (258), 539–571.

Feng, X., Li, Y. & Xing, Y. 2016 Analysis of mixed interior penalty discontinuous Galerkin methods for the Cahn-Hilliard equation and the Hele-Shaw flow. *SIAM J. Numer. Anal.* **54** (2), 825–847.

Feng, X. & Wise, S. 2012 Analysis of a Darcy-Cahn-Hilliard diffuse interface model for the Hele-Shaw flow and its fully discrete finite element approximation. *SIAM J. Numer. Anal.* **50** (3), 1320–1343.

Gal, C. G. & Grasselli, M. 2011 Instability of two-phase flows: a lower bound on the dimension of the global attractor of the Cahn-Hilliard-Navier-Stokes system. *Phys. D* **240** (7), 629–635.

García-Cervera, C. J. & Joo, S. 2012 Analytic description of layer undulations in smectic a liquid crystals. *Arch. Ration. Mech. Anal.* **203** (1), 1–43.

García-Cervera, C. J. & Joo, S. 2015 Reorientation of smectic a liquid crystals by magnetic fields. *Discrete Contin. Dyn. Syst. Ser. B* **20** (7), 1983–2000.

Garton, C. G. & Krasucki, Z. 1964 Bubbles in insulating liquids: Stability in an electric field. *Proc. R. Soc. Lond. A* **280** (1381), 211–226.

de Gennes, P. G. & Prost, J. 1993 *The Physics of Liquid Crystals*, 2nd edn. Oxford, UK: Oxford Science Publications.

Ghaffari, A., Hashemabadi, S. H. & Bazmi, M. 2015 CFD simulation of equilibrium shape and coalescence of ferrofluid droplets subjected to uniform magnetic field. *Colloids Surf. A* **481**, 186–198.

Guo, Z., Lin, P. & Lowengrub, J. S. 2014 A numerical method for the quasi-incompressible Cahn-Hilliard-Navier-Stokes equations for variable density flows with a discrete energy law. *J. Comput. Phys.* **276**, 486–507.

Hartshorne, H., Backhouse, C. J. & Lee, W. E. 2004 Ferrofluid-based microchip pump and valve. *Sensor Actuators B* **99** (2-3), 592–600.

Hatch, A., Kamholz, A. E., Holman, G., Yager, P. & Böhringer, K. F. 2001 A ferrofluidic magnetic micropump. *J. Microelectromech. S.* **10** (2), 215–221.

Helfrich, W. 1970 Deformation of cholesteric liquid crystals with low threshold voltage. *Appl. Phys. Lett.* **17** (12), 531–532.

Hua, J., Lim, L. K. & Wang, C. H. 2008 Numerical simulation of deformation/motion of a drop suspended in viscous liquids under influence of steady electric fields. *Phys. Fluids* **20** (11), 113302.

Hurault, J. P. 1973 Static distortions of a cholesteric planar structure induced by magnetic or ac electric fields. *J. Chem. Phys.* **59** (4), 2068–2075.

Hyon, Y., Kwak, D. & Liu, C. 2009 Energetic Variational Approach in Complex Fluids : Maximum Dissipation Principle. *Discrete Contin. Dyn. Syst. Ser. A* **26** (4), 1291–1304.

Jacqmin, D. 1999 Calculation of two-phase navierstokes flows using phase-field modeling. *J. Comput. Phys.* **155** (1), 96–127.

Ki, H. 2010 Level set method for two-phase incompressible flows under magnetic fields. *Comput. Phys. Comm.* **181** (6), 999–1007.

Kim, J. 2012 Phase-field models for multi-component fluid flows. *Comm. Comput. Phys* **12** (3), 613–661.

Kim, J., Kang, K. & Lowengrub, J. 2004 Conservative multigrid methods for Cahn-Hilliard fluids. *J. Comput. Phys.* **193** (2), 511–543.

Kim, J. & Lowengrub, J. 2005 Phase field modeling and simulation of three-phase flows. *Interfaces Free Bound.* **7** (4), 435–466.

Kleman, M. 1983 *Points, Lines, and Walls in Liquid Crystals, Magnetic Systems, and Various Ordered Media*. Chichester, New York: John Wiley.

Korlie, M. S., A., Nita, B. G., Stevens, J. G., Trubatch, Trubatch, A. D. & Yecko, P. 2008 Modeling bubbles and droplets in magnetic fluids. *J. Phys. Condens. Matter* **20** (20), 204143.

Kose, A. R., Fischer, B., Mao, L. & Koser, H. 2009 Label-free cellular manipulation and

sorting via biocompatible ferrofluids. *Proc. Natl. Acad. Sci. U. S. A.* **106** (51), 21478–21483.

Lanauze, J. A., Walker, L. M. & Khair, A. S. 2015 Nonlinear electrohydrodynamics of slightly deformed oblate drops. *J. Fluid Mech.* **774**, 245–266.

Lange, A., Gollwitzer, C., Maretzki, R., Rehberg, I. & Richter, R. 2016 Retarding the growth of the rosensweig instability unveils a new scaling regime. *Phys. Rev. E* **93**, 043106.

Lee, J., Park, J. K., Hong, J., Lee, S. J., Kang, K. H. & Hwang, H. J. 2014 Nonlinear oscillations of a sessile drop on a hydrophobic surface induced by ac electrowetting. *Phys. Rev. E* **90**, 033017.

Li, J., Renardy, Y. Y. & Renardy, M. 2000 Numerical simulation of breakup of a viscous drop in simple shear flow through a volume-of-fluid method. *Phys. Fluids* **12** (2), 269–282.

Lim, C. Y. & Lam, Y. C. 2014 Phase-field simulation of impingement and spreading of micro-sized droplet on heterogeneous surface. *Microfluid. Nanofluid.* **17** (1), 131–148.

Lin, F. & Pan, X. 2007 Magnetic field-induced instabilities in liquid crystals. *SIAM J. Math. Anal.* **38** (5), 1588–1612.

Lin, F. H. & Liu, C. 1995 Nonparabolic dissipative systems modeling the flow of liquid crystals. *Commun. Pur. Appl. Math.* **48**, 501–537.

Lin, F. H. & Liu, C. 2001 Static and dynamic theories of liquid crystals. *J. Part. Diff. Eq.* **14**, 289–330.

Lin, Y., Skjetne, P. & Carlson, A. 2012 A phase field model for multiphase electro-hydrodynamic flow. *Int. J. Multiphas Flow* **45**, 1–11.

Liu, C. & Shen, J. 2003 A phase field model for the mixture of two incompressible fluids and its approximation by a Fourier-spectral method. *Phys. D* **179** (3-4), 211–228.

Liu, J., Lawrence, E. M., Wu, A., Ivey, M. L., Flores, G. A., Javier, K., Bibette, J. & Richard, J. 1995 Field-induced structures in ferrofluid emulsions. *Phys. Rev. Lett.* **74**, 2828–2831.

Liu, J., Tan, S. H., Yap, Y. F., Ng, M. & Nguyen, N. T. 2011 Numerical and experimental investigations of the formation process of ferrofluid droplets. *Microfluid. Nanofluid.* **11** (2), 177–187.

Lowengrub, J. & Truskinovsky, L. 1998 Quasi-incompressible Cahn-Hilliard fluids and topological transitions. *R. Soc. Lond. Proc. Ser. A* **454** (1978), 2617–2654.

Mao, L. & Koser, H. 2005 Ferrohydrodynamic pumping in spatially traveling sinusoidally time-varying magnetic fields. *J. Magn. Magn. Mater.* **289**, 199–202.

Mefford, O. T., Woodward, R. C., Goff, J. D., Vadala, T. P., St. Pierre, T. G., Dailey, J. P. & Riffle, J. S. 2007 Field-induced motion of ferrofluids through immiscible viscous media: Testbed for restorative treatment of retinal detachment. *J. Magn. Magn. Mater.* **311** (1 SPEC. ISS.), 347–353.

Menech, M. De, Garstecki, P., Jousse, F. & Stone, H. A. 2008 Transition from squeezing to dripping in a microfluidic T-shaped junction. *J. Fluid Mech.* **595**, 141–161.

Miehe, C., Hofacker, M. & Welschinger, F. 2010 A phase field model for rate-independent crack propagation: Robust algorithmic implementation based on operator splits. *Comput. Methods Appl. Mech. Eng.* **199**, 2765–2778.

Müller-Fischer, N., Tobler, P., Dressler, M., Fischer, P. & Windhab, E. J. 2008 Single bubble deformation and breakup in simple shear flow. *Exp. Fluids* **45** (5), 917–926.

Napoli, G. & Nobili, A. 2009 Mechanically induced Helfrich-Hurault effect in lamellar systems. *Phys. Rev. E* **80** (3), 031710.

Nganguia, H., Young, Y. N., Layton, A. T., Lai, M. C. & Hu, W. F. 2016 Electrohydrodynamics of a viscous drop with inertia. *Phys. Rev. E* **93**, 053114.

Nochetto, R. H., Salgado, A. J. & Tomas, I. 2016 A diffuse interface model for two-phase ferrofluid flows. *Comput. Methods Appl. Mech. Engrg.* **309**, 497–531.

Nochetto, R. H., Salgado, A. J. & Walker, S. W. 2014 A diffuse interfce model for electrowetting with moving contat lines. *Math. Models Methods Appl. Sci.* **24** (1), 67–111.

Odenbach, S. 2004 Recent progress in magnetic fluid research. *J. Phys. Condens. Matter* **16** (32), R1135–R1150.

Onsager, L. 1931*a* Reciprocal relations in irreversible processes I. *Phys. Rev.* **37**, 405–426.

Onsager, L. 1931*b* Reciprocal relations in irreversible processes. II. *Phys. Rev.* **38**, 2265–2279.

Paknemat, H., Pishevar, A. R. & Pournaderi, P. 2012 Numerical simulation of drop deformations and breakup modes caused by direct current electric fields. *Phys. Fluids* **24** (10), 102101.

Pal, S., Datta, A., Sen, S., Mukhopdhyay, A., Bandopadhyay, K. & Ganguly, R. 2011 Characterization of a ferrofluid-based thermomagnetic pump for microfluidic applications. *J. Magn. Magn. Mater.* **323** (21), 2701–2709.

Patlazhan, S., Vagner, S. & Kravchenko, I. 2015 Steady-state deformation behavior of confined composite droplets under shear flow. *Phys. Rev. E* **91**, 063002.

Pillai, R., Berry, J. D., Harvie, D. J. E. & Davidson, M. R. 2015 Electrolytic drops in an electric field: A numerical study of drop deformation and breakup. *Phys. Rev. E* **92**, 013007.

Qian, T., Wang, X. & Sheng, P. 2006 A variational approach to the moving contact line hydrodynamics. *J. Fluid Mech.* **564**, 333–360.

Raj, K., Moskowitz, B. & Casciari, R. 1995 Advances in ferrofluid technology. *J. Magn. Magn. Mater.* **149** (1-2), 174–180.

Rinaldi, C. & Zahn, M. 2002 Effects of spin viscosity on ferrofluid flow profiles in alternating and rotating magnetic fields. *Phys. Fluids* **14**, 2847–2870.

Rosensweig, R. E. 1985 *Ferrohydrodynamics*, , vol. 14. Cambridge University Press.

Rosensweig, R. E. 1987 Magnetic fluids. *Ann. Rev. Fluid Mech.* **19**, 437–461.

Rosensweig, R. E. 2002 Basic equations for magnetic fluids with internal rotations, in Ferrofluids: Magnetically controllable fluids and their applications. *S. Odenbach, ed., Lecture Notes in Physics, Springer-Verlag* **46**, 61–84.

Rosensweig, R. E. 2007 Stress boundary-conditions in ferrohydrodynamics. *Ind. Eng. Chem. Res.* **46**, 6113–6117.

Rosenthal, A. D., Rinaldi, C., Franklin, T. & Zahn, M. 2004 Torque measurement in spin-up flow of ferro fluids. *J. Fluids. Engr.* **126**, 198–205.

Rowghanian, P., Meinhart, C. D. & Campàs, O. 2016 Dynamics of ferrofluid drop deformations under spatially uniform magnetic fields. *J. Fluid Mech.* **802**, 245–262.

Salipante, P. F. & Vlahovska, P. M. 2010 Electrohydrodynamics of drops in strong uniform dc electric fields. *Phys. Fluids* **22** (11), 112110.

Self, R. H., Please, C. P. & Sluckin, T. J. 2002 Deformation of nematic liquid crystals in an electric field. *Euro. J. Appl. Math.* **13**, 1–23.

Seric, I., Afkhami, S. & Kondic, L. 2014 Interfacial instability of thin ferrofluid films under a magnetic field. *J. Fluid Mech.* **755**, 1–12.

Shen, J. & Yang, X. 2009 An efficient moving mesh spectral method for the phase-field model of two-phase flows. *J. Comput. Phys.* **228** (8), 2978–2992.

Shen, J. & Yang, X. 2015 Decoupled, energy stable schemes for phase-field models of two-phase incompressible flows. *SIAM J. Numer. Anal.* **53** (1), 279–296.

Sherwood, J. D. 1988 Breakup of fluid droplets in electric and magnetic fields. *J. Fluid Mech.* **188**, 133–146.

Sherwood, J. D. 1991 The deformation of a fluid drop in an electric field: a slender-body analysis. *J. Phys. A* **24** (17), 4047.

Shliomis, M. I. 1972 Effective viscosity of magnetic suspensions. *Soviet Phys. Jetp* **34** (6), 1291–1294.

Shliomis, M. I. 2002 Ferrohydrodynamics: Retrospective and issues. *in: S. Odenbach (Ed.), Ferrofluids: Magnetically Controllable Fluids and their Applications, Lecture Notes in Physics, Springer-Verlag* pp. 85–111.

Sofonea, V., Früh, W. G. & Cristea, A. 2002 Lattice boltzmann model for the simulation of interfacial phenomena in magnetic fluids. *J. Magn. Magn. Mater.* **252**, 144–146.

Stephen, M. J. & Straley, J. P. 1974 Physics of liquid crystals. *Rev. Mod. Phys.* **46**, 617–704.

Tan, S. H. & Nguyen, N. T. 2011 Generation and manipulation of monodispersed ferrofluid emulsions: The effect of a uniform magnetic field in flow-focusing and T-junction configurations. *Phys. Rev. E* **84**, 036317.

Tan, S. H., Nguyen, N. T., Yobas, L. & Kang, T. G. 2010 Formation and manipulation of ferrofluid droplets at a microfluidic T-junction. *J. Micromech. Microeng.* **20** (4), 045004.

Torza, S., Cox, R. G. & Mason, S. G. 1971 Electrohydrodynamic deformation and burst of liquid drops. *Philos. Tr. Soc. A* **269** (1198), 295–319.

Wang, C. & Wise, S. M. 2011 An energy stable and convergent finite-difference scheme for the modified phase field crystal equation. *SIAM J. Numer. Anal.* **49** (3), 945–969.

Wang, X., Qian, T. & Sheng, P. 2008 Moving contact line on chemically patterned surfaces. *J. Fluid Mech.* **605**, 59–78.

Wise, S. 2010 Unconditionally stable finite difference, nonlinear multigrid simulation of the Cahn-Hilliard-Hele-Shaw system of equations. *J. Sci. Comput.* **44** (1), 38–68.

Wu, Y., Fu, T., Ma, Y. & Li, H. Z. 2013 Ferrofluid droplet formation and breakup dynamics in a microfluidic flow-focusing device. *Soft Matter* **9**, 9792–9798.

Xi, H. D., Guo, W., Leniart, M., Chong, Z. Z. & Tan, S. H. 2016 AC electric field induced droplet deformation in a microfluidic T-junction. *Lab Chip* **16**, 2982–2986.

Yang, Q., Li, B. Q. & Ding, Y. 2013 3D phase field modeling of electrohydrodynamic multiphase flows. *Int. J. Multiphas Flow* **57**, 1–9.

Yang, X., Feng, J. J., Liu, C. & Shen, J. 2006 Numerical simulations of jet pinching-off and drop formation using an energetic variational phase-field method. *J. Comput. Phys.* **218** (1), 417–428.

Yecko, P. 2009 Stability of layered channel flow of magnetic fluids. *Phys. Fluids* **21** (3), 034102.

Yecko, P. 2010 Effect of normal and parallel magnetic fields on the stability of interfacial flows of magnetic fluids in channels. *Phys. Fluids* **22** (2), 1–8.

Yue, P., Feng, J., Liu, C. & Shen, J. 2004 A diffuse-interface method for simulating two-phase flows of complex fluids. *J. Fluid Mech.* **515**, 293–317.

Zahn, M. & Greer, D. R. 1995 Ferrohydrodynamic pumping in spatially uniform sinusoidally time-varying magnetic fields. *J. Magn. Magn. Mater.* **149**, 165–173.

Zelazo, R. E. & Melcher, J. R. 1969 Dynamics and stability of ferrofluids: surface interactions. *J. Fluid Mech.* **39** (01), 1–24.

Zeng, J., Deng, Y., Vedantam, P., Tzeng, T. R. & Xuan, X. 2013 Magnetic separation of particles and cells in ferrofluid flow through a straight microchannel using two offset magnets. *J. Magn. Magn. Mater.* **346**, 118–123.

Zhao, J., Yang, X., Shen, J. & Wang, Q. 2016 A decoupled energy stable scheme for a hydrodynamic phase-field model of mixtures of nematic liquid crystals and viscous fluids. *J. Comput. Phys.* **305**, 539C556.

Zhu, J., Liang, L. & Xuan, X. 2012 On-chip manipulation of nonmagnetic particles in paramagnetic solutions using embedded permanent magnets. *Microfluid. Nanofluid.* **12** (1-4), 65–73.